



# Transonic Panel Flutter in Accelerating or Decelerating Flow Conditions

Anastasia Shishaeva\* and Vasily Vedenev†

*Lomonosov Moscow State University, 119192 Moscow, Russia*

and

Andrey Aksenov‡ and Gennady Sushko§

*Tesis LTD, 127083 Moscow, Russia*

DOI: 10.2514/1.J056217

**Nonlinear panel flutter oscillations at transonic and low supersonic flow speed demonstrate rich panel dynamics, which includes bifurcations of the limit cycle, coexisting of different limit cycles, and nonperiodic oscillations. Passing through the range of transonic Mach numbers to supersonic cruise speed should be sufficiently fast to avoid significant fatigue damage. In this study, the sequence of bifurcations of limit cycles when the flow speed is continuously increasing or decreasing is analyzed. The evolution of limit-cycle oscillations is carefully studied. It is shown that the most dangerous oscillation regimes, high-frequency periodic or nonperiodic oscillations, are suppressed if the flow acceleration is sufficiently fast. However, first-mode limit cycle and limit cycle involving internal 1:2 resonance are not affected by the flow acceleration, such that lower accumulation of the fatigue damage in fast accelerating flow is possible only because of fewer cycles of oscillations, but not because of the decrease of the limit-cycle amplitude.**

## I. Introduction

**F**LUTTER of various structures of flight vehicles, such as control surfaces and skin panels, at subsonic and high supersonic flow speed has been studied over many decades and currently is well understood (except for such features as boundary layer and aerodynamic heating effect at high speeds). Typically, the flutter boundary can be calculated through linear structural and aerodynamic models, and the growth of perturbations in the flutter regime yields the formation of certain limit-cycle oscillations that can be analyzed through appropriate nonlinear models. In many cases, only structural nonlinearity is essential, and the linear aerodynamic model still gives good accuracy.

On the contrary, flutter at transonic flow (including some portion of low supersonic speeds) is still a challenging problem. First, aerodynamic nonlinearity is essential even at small amplitudes (i.e., it cannot be neglected in the calculation of flutter boundary [1]). Second, structures of flight vehicles are subject to “transonic dip”, associated with negative aerodynamic damping of natural modes, where the instability region significantly expands, and flutter is possible for very small flow density, which is attained at high altitudes [2,3]. Third, several natural modes grow simultaneously, which yields complex nonlinear dynamics of the structure: nonuniqueness of limit cycles and possible nonperiodic oscillations [4,5].

Because the range of Mach numbers occupied by the transonic dip is bounded and usually is within  $0.95 < M < 1.4$  range, the flight vehicle should pass it as quickly as possible to avoid accumulation of fatigue damage. However, it is still not known how the acceleration of the flight vehicle will impact limit-cycle oscillations.

In this paper, we analyze this question of the simplest aeroelastic model representing flutter of a skin panel, namely, a flat elastic plate in a uniform airflow. This classical panel flutter problem has been

studied in the 1950–1970s in numerous papers, where linear piston theory was employed for modeling high-speed supersonic flow [6–11]. The interest in this problem was renewed in the 2000s, when several aeroelastic solvers based on full Euler or Reynolds-averaged Navier–Stokes equations were developed by different groups and showed their capability of solving the panel flutter problem at transonic and low supersonic speed in linear [12,13] and nonlinear [5,14–21] formulations.

Note that single mode flutter, which is caused by negative aerodynamic damping dominating in this range of speeds, can be significantly affected by the boundary layer over the panel surface (unlike coupled-mode flutter at high supersonic speeds). Although zero-gradient boundary layers reduce the flutter region in the parameter space [15,16,18,19,22–25], boundary layers over concave walls can be essentially destabilizing [26,27]. In this paper, the boundary layer is neglected for simplicity, and only inviscid fluid–structure interaction mechanism is studied.

In our preceding paper [5], we considered the development of nonlinear panel flutter oscillations at constant subsonic, transonic, and supersonic speeds. We showed that the panel oscillations experience various bifurcations when changing the Mach number of the flow. Besides well-known transitions from stability to static divergence at  $M < 1$  (pitchfork bifurcation) and from divergence to flutter at  $M \approx 1$  (Hopf bifurcation), we found bifurcations of limit-cycle oscillations at  $M > 1$ . Namely, at small supersonic speeds, the limit-cycle oscillations are symmetric and consist of the first mode only. At  $M \approx 1.12$ , the second mode can be excited, and a new limit cycle, which includes internal 1:2 resonance between the first and the second modes, appears (the existence of this limit cycle was shown in a closed form in [28,29]). Next, at  $M = 1.33$ , higher modes are excited, and oscillations take the form of either regular or irregular higher-mode oscillations. However, after passing the most destructive higher-mode regime, at  $M = 1.5$ , the oscillations return to the first-mode limit cycle, which dies out at  $M \approx 1.67$ . For  $M > 1.67$ , the plate stays stable, until the coupled-mode flutter occurs at much higher speed.

In this paper, we reinvestigate this problem by modeling continuously accelerating and decelerating air speed and have two goals in mind. First, this approach allows better understanding of the bifurcations of the limit cycle and shows their evolution in more details. Second, a more practical goal is to investigate the panel oscillations at transient regimes, especially at high accelerations, and to explore the possibility of avoiding the most destructive limit-cycle oscillations, or full suppression of flutter, if the transonic regime is passed sufficiently fast.

Received 12 April 2017; revision received 29 September 2017; accepted for publication 4 December 2017; published online 23 January 2018. Copyright © 2017 by Anastasia Shishaeva, Vasily Vedenev, Andrey Aksenov, and Gennady Sushko. Published by the American Institute of Aeronautics and Astronautics, Inc., with permission. All requests for copying and permission to reprint should be submitted to CCC at [www.copyright.com](http://www.copyright.com); employ the ISSN 0001-1452 (print) or 1533-385X (online) to initiate your request. See also AIAA Rights and Permissions [www.aiaa.org/randp](http://www.aiaa.org/randp).

\*Lead Researcher, Institute of Mechanics, 1, Michurinskii Prosp.

†Head of Lab, Institute of Mechanics, 1, Michurinskii prosp.

‡Technical Director, 18, Yunnatov str.

§Engineer, 18, Yunnatov str.

## II. Formulation of the Problem and Method of Solution

We investigate the nonlinear evolution of small perturbations of a clamped elastic plate (which represents a skin panel of a flight vehicle) in accelerating or decelerating airflow. The air can flow either over one side of the panel, as shown in Fig. 1a (this model represents “classical” flutter problem), or over both sides (Fig. 1b), but with half of the density of the one-side flow. The latter case represents the symmetrical problem, which aims to understand the source of nonsymmetry in the panel oscillations at some regimes; primarily, we will consider the classical one-side flow.

The simulation domain is shown in Fig. 2. The size of the flow domain is chosen so that the top and bottom boundaries are located far enough from the plate to not affect the flow near the plate, and the latter can be considered as interacting with the unbounded flow. The air is modeled as inviscid perfect gas (i.e., the boundary layer over the plate is neglected). To enforce this condition, we specify a free-slip condition along the surface of the bent plate. Small artificial viscosity of the flow is added to stabilize the numerical solution; it was checked that the viscosity is small enough to not affect the flow.

Nonreflecting boundary conditions are specified over external boundaries of the flow domain (i.e., inlet, outlet, top, and bottom boundaries). Namely, depending on whether the flow enters or leaves the domain, one of the Riemann invariants is specified based on far-field parameters of the flow. This boundary condition provides no reflection of incident waves from top and bottom boundaries; to ensure this, the convergence in the domain size was additionally checked in a special series of runs. Far-field flow parameters are as follows: constant pressure  $p = 100$  kPa (one-side) or 50 kPa (two-side flow) and constant temperature  $T = 273$  K (the same for both flow configurations).

Far-field flow velocity is a linear function of time, so that the Mach number is

$$M(t) = M_1 + (M_2 - M_1)(t/T) \quad (1)$$

for the accelerating flow and

$$M(t) = M_2 - (M_2 - M_1)(t/T) \quad (2)$$

for the decelerating flow. In all cases studied, we consider initial and final Mach numbers  $M_1 = 0.7$  and  $M_2 = 1.7$ . Various values of the time period  $T$ , which characterizes the acceleration (deceleration) of the flow, are considered.

We consider perfect gas model; hence, because  $p = \rho RT$ , two times difference in pressure between two flow configurations yields two

times difference in density. If the flow perturbation is small, and Euler equations are linearized, this would provide the same pressure distribution over the plate for both flow configurations. However, nonlinear flow response is different; when the plate bends, say, upward, this yields shock waves over the top side of the plate and expansion waves over the bottom side, which produce different pressure distributions. That is why the difference between the two flow configurations is the aerodynamic nonlinearity, whereas the linear flow response and the structural linear and nonlinear responses are the same.

The plate is modeled by the nonlinear Mindlin plate model, with the elastic strains calculated through Koiter–Sanders shell theory. Its length is 0.3 m, the thickness is 0.001 m, and steel material properties are assigned: Young’s modulus  $E = 2 \times 10^{11}$  Pa, Poisson’s coefficient  $\nu = 0.3$ , and density  $\rho_m = 7800$  kg/m<sup>3</sup>. Note that, in dimensionless quantities, the combination of steel properties and air properties at normal condition is the same as for an aluminum plate in air at 11,000 m above sea level, so that results presented in this paper are also concerned with this case.

The plate is continuously excited by applying a small perturbing pressure along a small piece (of 0.005 m length) of the plate surface:  $p = \varepsilon \sin(2\pi\Omega t)$ , where  $\varepsilon = 1000$  Pa, and  $\Omega$  is the first natural frequency of the plate. Continuous excitation (unlike short initial disturbance [5]) is used to enforce each bifurcation immediately when the system is ready to bifurcate.

The problem is solved in two codes, FlowVision (modeling of the flow by the finite volume method) and Abaqus (modeling of the plate through the finite element method), coupled in both ways through the conventional serial staggered procedure. The flow mesh is shown in Fig. 3; its size is  $50 \times 494$  (one-side) and  $50 \times 772$  (two-side flow). The panel mesh consists of 60 finite elements. A detailed description of the numerical procedure, mesh, and time step convergence study as well as a validation of the solution can be found in our preceding paper [5]; they are omitted here for the sake of brevity.

In spite of apparent simplicity, the flow-plate dynamics is rather complex. An observation of the temporally changing plate shape takes a long time and is hard to analyze. That is why we investigate the plate motion by watching vertical deflection of a reference point plotted versus time (time series) as well as spectrum, phase portrait, and Poincaré map obtained from the time series of this point. The reference point is located at 0.22 m downstream of the leading edge of the elastic plate, which is approximately 3/4 of the plate length.

## III. Results of Calculations for Accelerating Flow

We analyzed the plate-flow dynamics for accelerations corresponding to  $T = 10, 7.5, 5, 2.5, 1,$  and  $0.5$  s, which represent

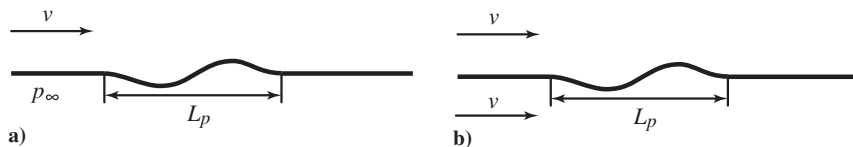


Fig. 1 Representations of a) one-side, and b) two-side airflow over an elastic plate.

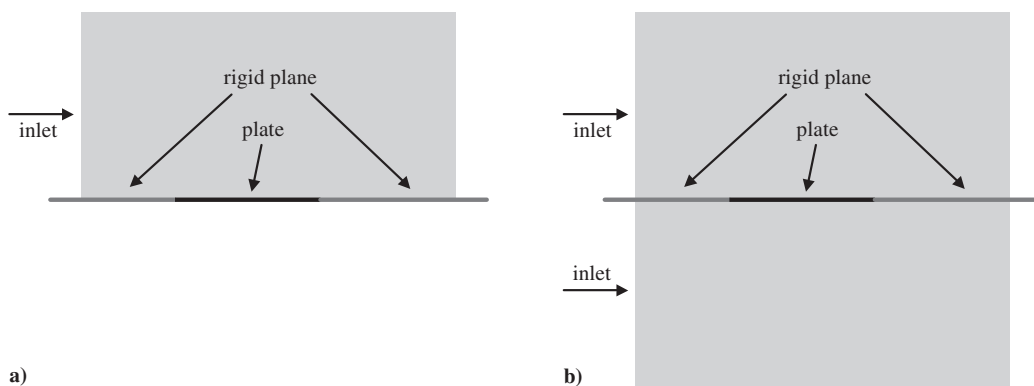


Fig. 2 Simulation domain for the case of a) one-side, and b) two-side airflow.

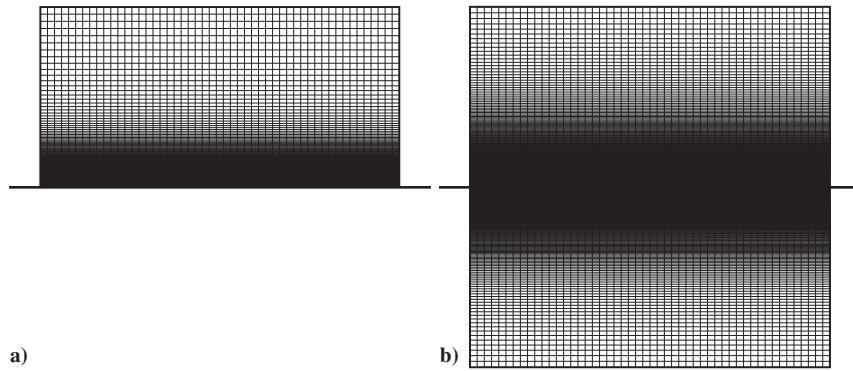


Fig. 3 Computational grid for the case of a) one-side, and b) two-side airflow.

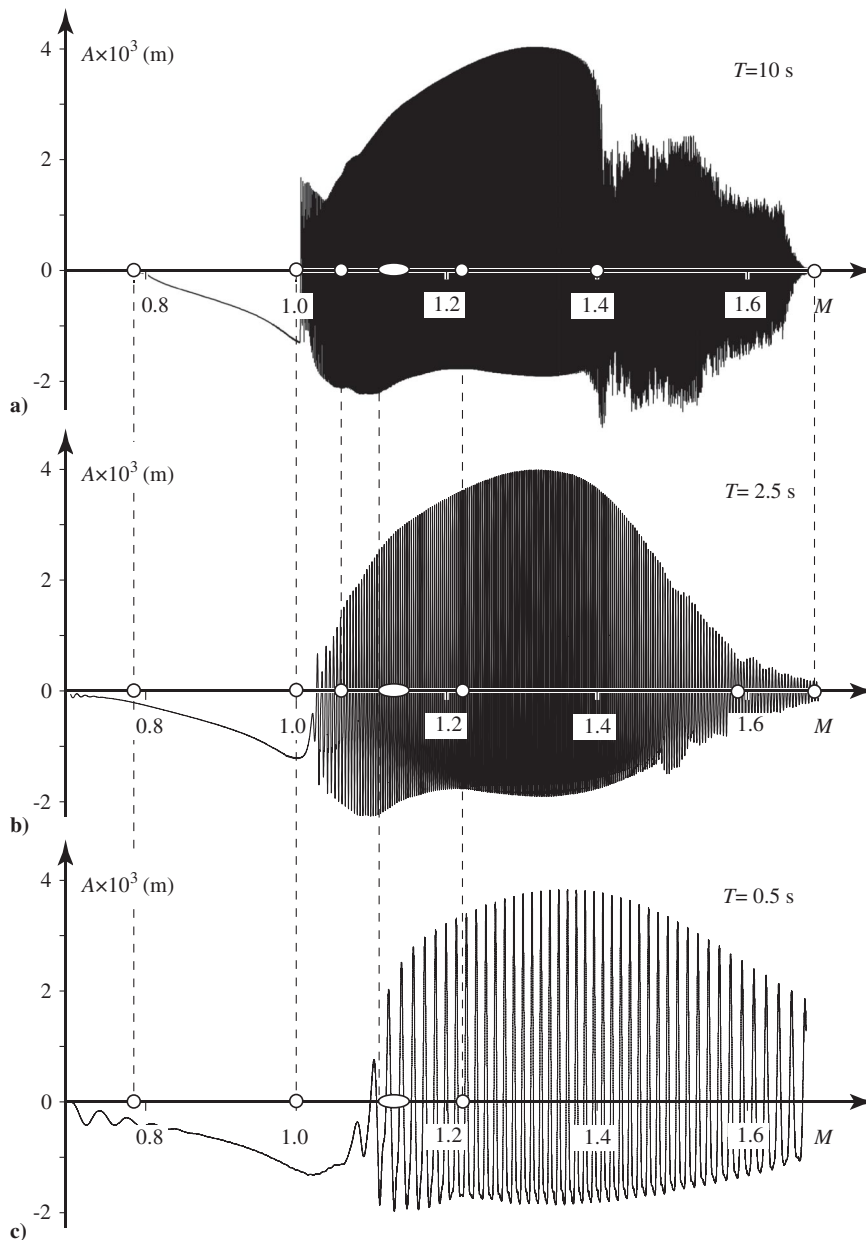
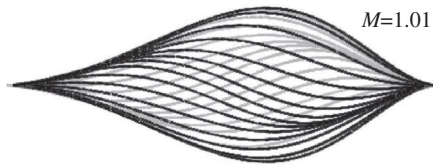


Fig. 4 Time series of the reference point deflection  $A$  for accelerating flow with a)  $T = 10$  s, b) 2.5 s, and c) 0.5 s. Position of each bifurcation is shown by a circle on the horizontal axis.

the acceleration range from very slow ( $T = 10$  s) to extremely fast ( $T = 0.5$  s). Results of calculations are shown in Fig. 4 and discussed later.

#### A. Slow Accelerations

At slow flow accelerations,  $T = 10, 7.5,$  and  $5$  s, the sequence of bifurcations in the plate dynamics is the same as at constant speeds [5].



**Fig. 5** Plate shape along the oscillation cycle after the Hopf bifurcation. Motion upward (black) and downward (gray).

A typical time history of the reference point deflection  $A$  is shown in Fig. 4a for  $T = 10$  s. The following changes in the plate dynamics are seen when the flow speed is increasing.

#### 1. Pitchfork Bifurcation at $M \approx 0.78$

At this Mach number, the panel becomes unstable; it is diverged from the flat state. Observations show that the static shape of the bent plate coincides with the first natural mode shape. When increasing  $M$ , the divergence amplitude increases, until the sonic speed is reached, where Hopf bifurcation occurs.

#### 2. Hopf Bifurcation at $M = 1.0$

Here, the first-mode limit cycle is born. Oscillations have a form of a forward-traveling wave, as shown in Fig. 5. Several first cycles of oscillations are far from harmonic; the plate motion is delayed in upward bent positions. For  $M$  just slightly higher than 1.0, delays rapidly disappear, and oscillations become more smooth (Fig. 6). It is seen that, in the case of one-side flow, the deflection of the plate bent upward and downward is nonsymmetric, whereas they are purely symmetrical for the two-side flow. Because the nonsymmetry of the one-side flow model is only in the aerodynamic nonlinearity, we conclude that this nonlinearity is responsible for the nonsymmetry of oscillations at  $M \approx 1.0$  in the case of one-side flow.

#### 3. Collapse of Twists at $M \approx 1.06$

When oscillations are just started at  $M = 1.0$ , they have a form of pure forward-traveling wave. At higher  $M$ , twists of the oscillations appear near the trailing edge, which is seen in Fig. 7 in the rear part of the plate as well as in the time series for the reference point shown in Fig. 8 (arrows show the directions of twist motions when  $M$  increases). With the increase of Mach number, positions of twists move to each other and collapse at  $M \approx 1.06$ . After the collapse, the oscillations become smooth and look more like standing-wave oscillations, with much less presence of the forward-traveling wave component (Fig. 7).

Phase portraits shown in Fig. 8 provide the most clear evidence of this bifurcation. Before the bifurcation, the phase portrait has two twists, which tend to each other when  $M$  is increasing. At the

bifurcation point, they collide and disappear, the and phase portrait becomes smooth.

Note that, at this bifurcation, the spatial modal structure of oscillations is not changed; the first natural mode is dominant.

#### 4. Birth of the 1:2 Resonant Limit Cycle at $1.11 < M < 1.15$

Vedenev [28,29] considered a closed-form solution for limit-cycle oscillations of the plate and showed that, although at small supersonic speeds, only first-mode limit cycle is possible, for slightly higher  $M$ , another limit cycle is born, which consists of the first and the second modes being in internal 1:2 resonance. Later, Shishaeva et al. [5] observed this resonant limit cycle in their numerical simulation of nonlinear oscillations at constant flow speed. The resonant limit cycle coexists with the first mode nonresonant limit cycle, such that the choice of the limit cycle depends on the initial perturbation. After the switch to the resonant limit cycle, the plate oscillation shape (Fig. 9), time series, and the phase portrait (Fig. 10) become nonsymmetric. For the two-side flow (Fig. 10), there is a certain point  $M \approx 1.14$ , which corresponds to the switch to nonsymmetrical time series. The same occurs for the one-side flow; however, because the oscillations are already slightly nonsymmetrical before this bifurcation due to nonsymmetric aerodynamic nonlinearity, the transition to resonant limit cycle is smooth (Fig. 10a), and no certain bifurcation point can be pointed out.

Note that, although before this bifurcation the traveling-wave component of the oscillations was always forward-traveling, in the resonant limit cycle, it is forward-traveling when the plate moves up but backward-traveling when the plate moves down (Fig. 9). This effect is the result of the presence of the second mode, which has two times higher frequency.

#### 5. Bifurcation of Resonant Limit-Cycle Oscillations at $M \approx 1.22$

This bifurcation is very minor and was not noticed in the previous constant-speed study [5]. When passing through this bifurcation point, there is an evident increase of the noise level in the plate dynamics but no visible change in the oscillation shape. However, observation of the phase portrait in Fig. 11 (arrows show the directions of twist motions when  $M$  increases) shows a clear bifurcation of the phase trajectory at its left tip. Although the trajectory was smooth before this bifurcation, it has two twists after passing through the bifurcation point. When observing the time series (Fig. 4) for small acceleration, the change in the oscillation is hardly seen; however, it becomes more pronounced when the acceleration is increased. Especially, for  $T = 0.5$  s, there is a clear change in the bottom portion of the time series; delays, which correspond to twists of the phase trajectory, are seen in Fig. 4c.

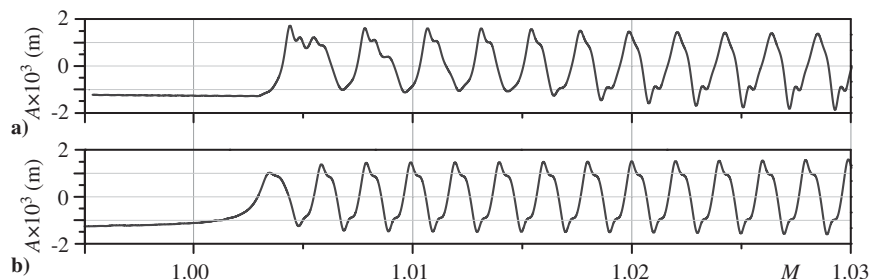


**Fig. 6** Time series of the reference point deflection during Hopf bifurcation: a) one-side, and b) two-side flow.

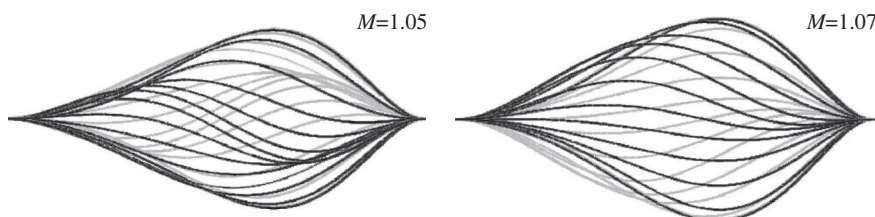


**Fig. 7** Plate shape along the oscillation cycle before and after bifurcation 3. Motion upward (black) and downward (gray).

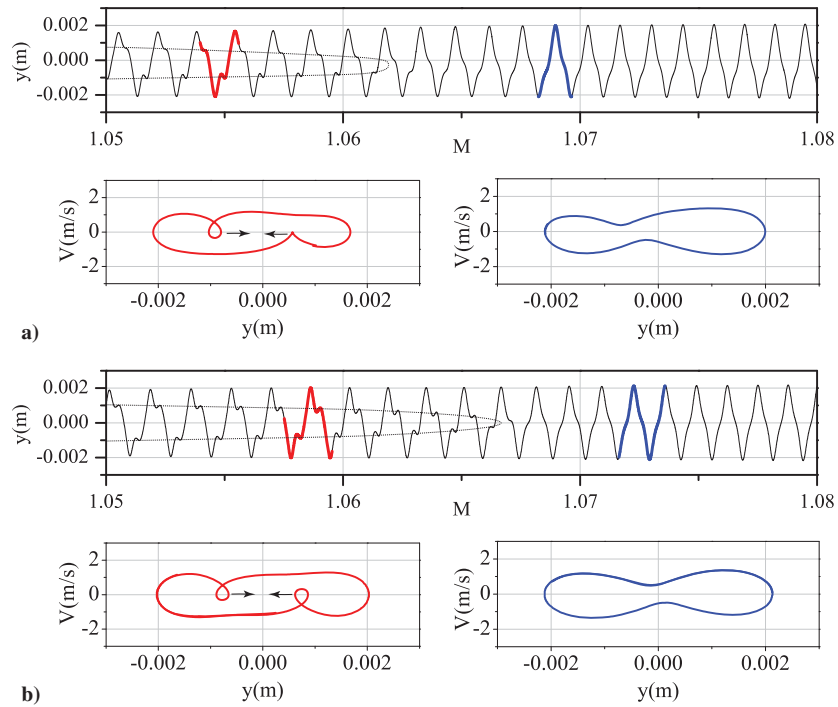


Fig. 8 Time series and the change of the phase portrait of the reference point deflection during bifurcation 3: a) one-side, and b) two-side flow.

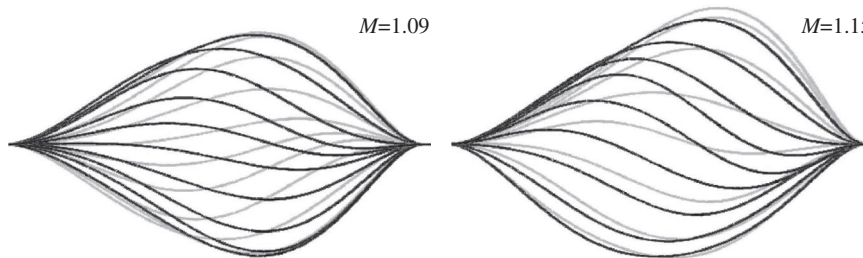


Fig. 9 Plate shape along the oscillation cycle before and after bifurcation 4. Motion upward (black) and downward (gray).

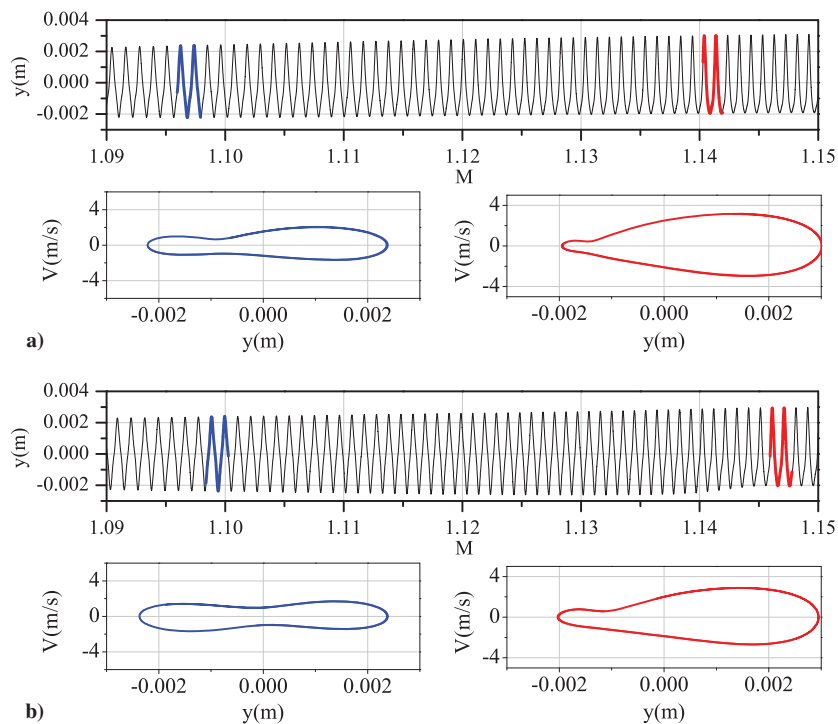
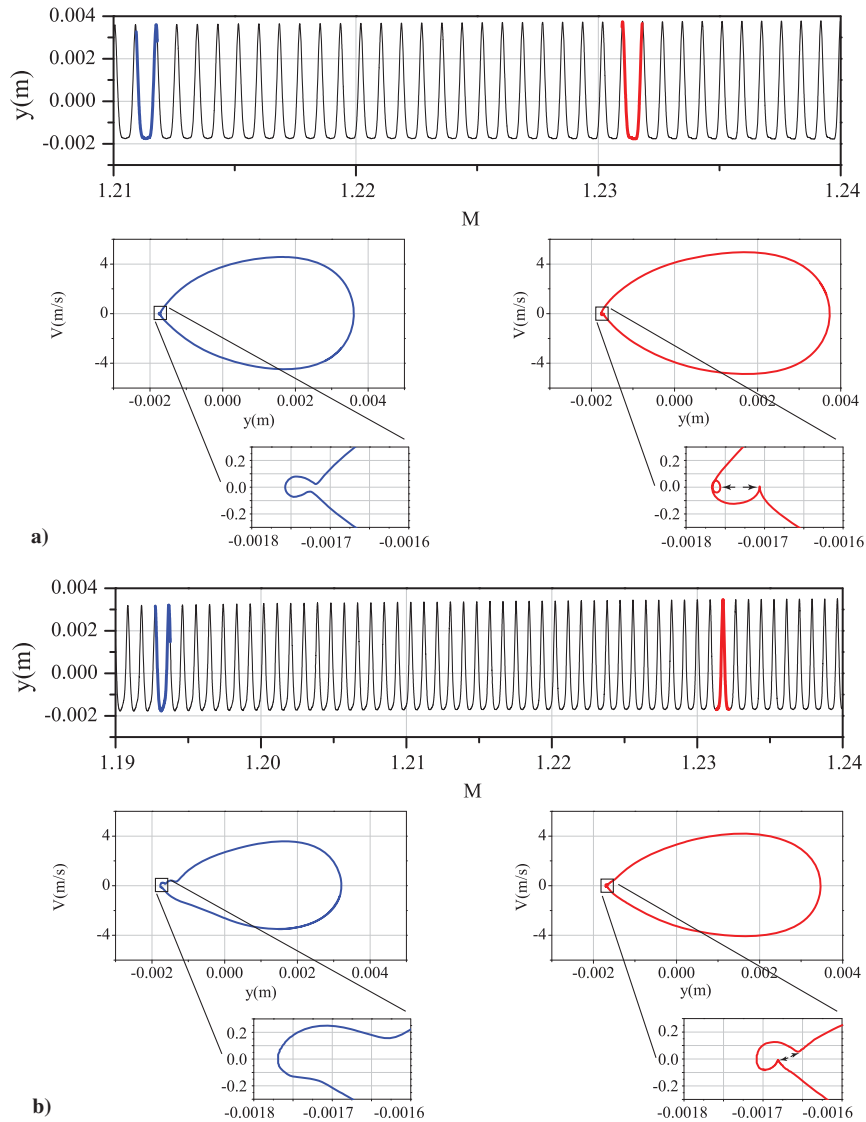


Fig. 10 Time series and change of the phase portrait of the reference point deflection during bifurcation 4: a) one-side, and b) two-side flow.



**Fig. 11** Time series and change of the phase portrait of the reference point deflection during bifurcation 5: a) one-side, and b) two-side flow.

#### 6. Transition from Resonant Limit Cycle to High-Frequency Nonperiodic Oscillations at $M \approx 1.4$

According to linear flutter boundaries [3], the first mode becomes damped when Mach number exceeds  $M \approx 1.4$ . Therefore, this mode cannot provide energy inflow into the plate from the flow and cannot anymore support the limit-cycle oscillations. However, higher modes stay linearly growing; they convey the energy from the flow to the plate, and their presence in the plate shape dramatically increases (Figs. 12 and 13). On the other hand, there is no clearly dominating mode; each one is growing and tends to establish its own limit cycle. Because of concurrence between multiple growing modes, no limit cycle corresponding to one certain mode is reached, and the process becomes chaoticlike, with spontaneous changes of the plate shape from the second to the sixth mode shapes. Note that, at constant-speed analysis [5], there is a small gap of Mach numbers near  $M \approx 1.4$ , where higher-mode limit cycle is established (both nonresonant fourth-mode limit cycle, and resonant second- and

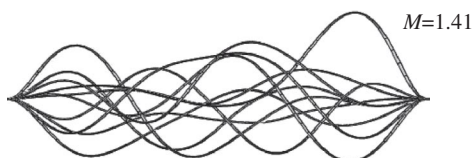


**Fig. 12** Plate shapes during nonperiodic oscillations.

fourth-mode limit cycle were observed); however, in accelerating flow, this gap is passed very quickly, and the oscillations become chaoticlike without any evidence of higher-mode limit cycles.

#### 7. Transition to Stability at $M \approx 1.69$

Starting from  $M \approx 1.65$ , high-frequency oscillations rapidly decay, and the plate is stabilized at  $M \approx 1.69$ . No further oscillations occur.

This sequence of bifurcation in the plate dynamics occurs at transonic and low supersonic speeds, where single-mode flutter in several modes is active. Note that all these bifurcations, including the third and the fifth, are present in constant-speed analysis, but the latter two were not noticed before [5].

After the plate stabilization, it stays flat while  $M \leq M_{cr} \approx 2.92$  [5]. At  $M > M_{cr}$ , the coupled-mode flutter occurs, which yields nonlinear limit-cycle oscillations with the plate shape composed of the first and the second natural mode shapes, and the plate stays fluttering for arbitrarily higher  $M$ . Because limit-cycle oscillations (LCOs) at coupled-mode flutter are well studied in the literature, we do not analyze them in this paper.

#### B. Moderate Accelerations

For faster flow acceleration,  $T = 2.5$ , time series is shown in Fig. 4b. It is clearly seen that the first five bifurcations are similar to

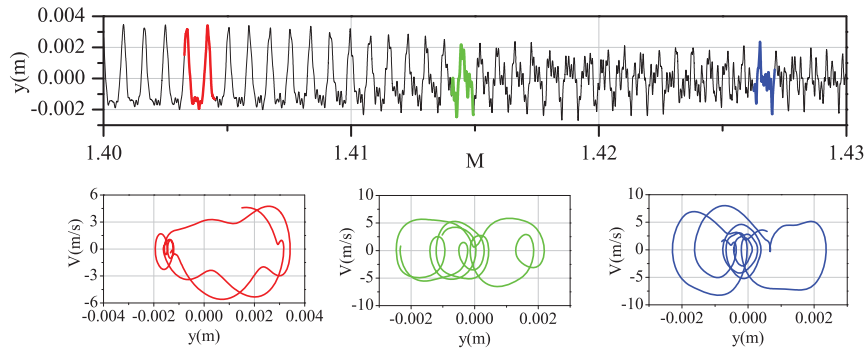


Fig. 13 Time series and the change of the phase portrait of the reference point deflection during bifurcation 6.

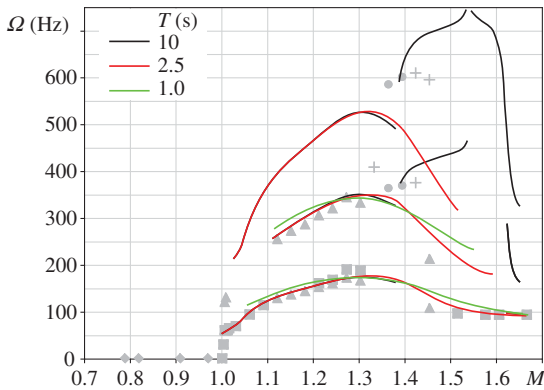


Fig. 14 Dominant frequencies in the oscillation spectrum vs  $M$  for accelerating flow. Symbols denote results for constant-speed flow [5]: divergence (◆), first-mode limit cycle (■), 1:2 resonant limit cycle (▲), high-frequency limit cycle (+), and nonperiodic oscillations (●).

those present at lower accelerations (Fig. 4a). However, transition to high-frequency periodic or nonperiodic oscillations does not occur. For  $M > 1.4$ , the amplitude of resonant limit cycle decreases. At  $M = 1.58$ , resonant oscillations are converted into nonresonant first-mode limit cycle. The amplitude continues decreasing, and the oscillations die out at  $M \approx 1.69$ .

The reason of the absence of high-frequency oscillations for these accelerations is their long formation period. As was noted by Shishaeva et al. [5] in their constant-speed study, high-frequency oscillations need much more time to develop than first-mode nonresonant or resonant limit cycles due to lower growth rates of higher modes. When the time period  $T$  decreases (i.e., flow acceleration increases), the range of Mach numbers where high-frequency oscillations occur becomes shorter and disappears at  $2.5 < T < 5$  s. For faster flow acceleration, Mach number leaves the region of high-frequency oscillations before they actually manifest themselves. That is why only first-mode and resonant limit cycles are observed.

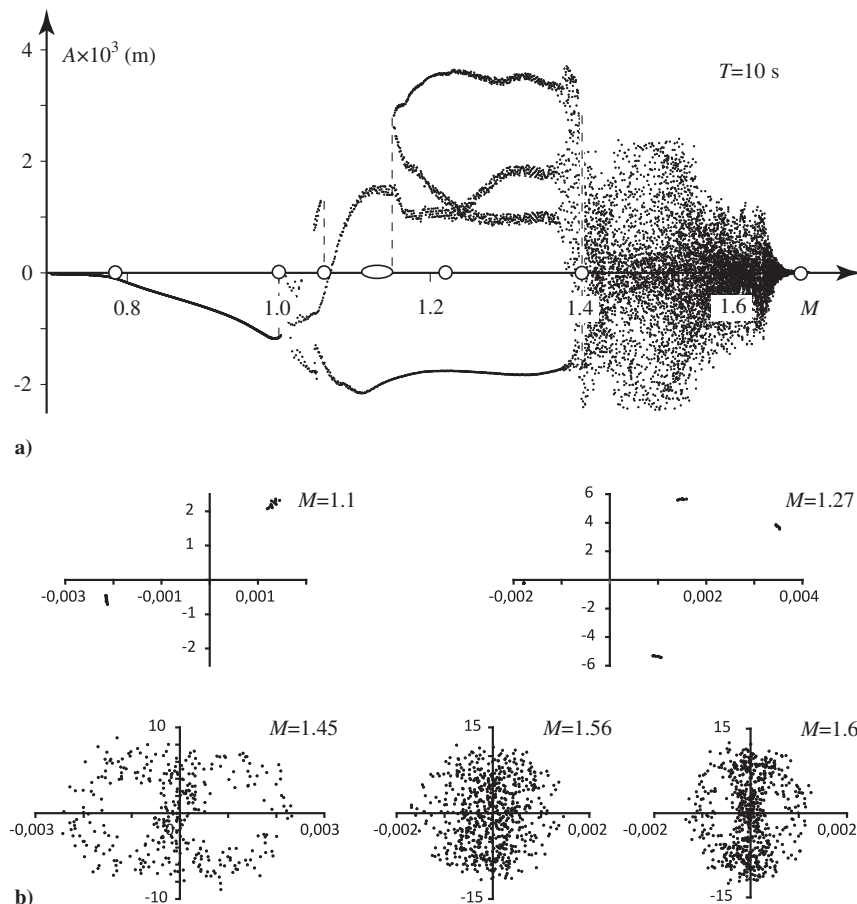


Fig. 15 Representations of a) position of point 1 at extrema of point 2 for accelerating flow,  $T = 10$  s, and b) corresponding Poincaré maps at various Mach numbers.

### C. Fast Accelerations

The time series for more significant accelerations,  $T = 1$  and  $0.5$  s (Fig. 4c), in general, follows the sequence of bifurcations similar to shown in Fig. 4b. It can only be noted that the oscillations do not convert from resonant to nonresonant at  $M \approx 1.58$ , at least in the range of analyzed Mach numbers. They also do not die out at  $M \approx 1.69$ ; despite no energy inflow from the air, the oscillations are continued as free and disappear at higher  $M$ .

Note that, for such high accelerations, the oscillations start not at  $M = 1$  but at  $M \approx 1.11$ , immediately in the form of resonant oscillations. This is caused by a small overpressurization above the plate due to continuous increase of the flow speed. In result, oscillations start slightly later than for larger  $T$ . For the two-side flow, overpressurization above and below the plate compensate each other, and calculations show that the oscillations start at  $M = 1$  even for the highest acceleration considered.

### D. Oscillation Frequency

Figure 14 shows dominant frequencies in the oscillation spectrum versus Mach number. It is seen that, at  $1 < M < 1.13$ , when the limit

cycle is nonresonant, only two frequencies being in 1:3 ratio are present in the spectrum. The first frequency corresponds to the first-mode oscillations, and the tripled frequency is an artifact of the cubic nonlinearity of the plate model (i.e., it does not correspond to its proper eigenmode). At the birth of the resonant limit cycle, a doubled frequency appears. It corresponds to the second-mode oscillations present in the plate shape as shown in Fig. 9. At  $M \approx 1.4$ , when nonperiodic oscillations occur for  $T = 10$  s, the spectrum shows the dominance of higher-mode frequencies, which are not in any simple ratio.

Faster accelerations show the absence of higher frequencies at  $M > 1.4$  so that no significant change of the spectrum occurs during the oscillation history.

### E. Poincaré Maps

A Poincaré map, which is a projection of infinite-dimension dynamics to a low-dimension phase space, is an effective tool for a detailed analysis of nonperiodic oscillations [30]. We will use a map definition similar to [30]; we will analyze a phase plane of the reference point, which will refer to as "point 1" when another point

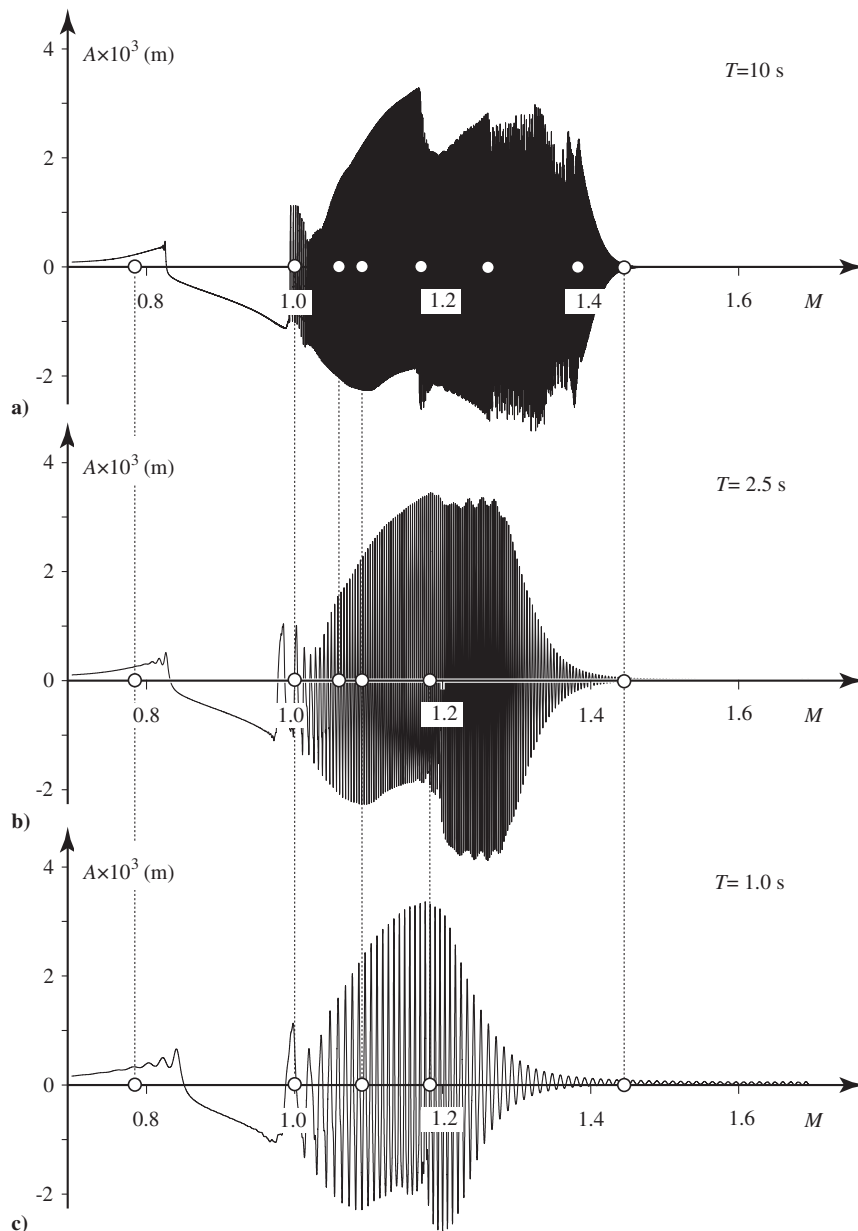


**Fig. 16** Time series of the reference point deflection  $A$  for decelerating flow with a)  $T = 10$  s, b)  $2.5$  s, and c)  $1.0$  s. Position of each bifurcation is shown by a circle on the horizontal axis.

that we will refer to as “point 2” reaches maximum or minimum deflection. In other words, point 2 is used to discretize time and point 1 to analyze the plate dynamics. Point 2 is located at 0.08 m downstream of the leading edge of the plate, which is approximately 1/4 of the plate length. Figure 15a shows deflection of point 1 when deflection of point 2 reaches its extremum. Most of the bifurcations of the plate dynamics are clearly seen in this plot; namely, besides the first two obvious bifurcations, the third bifurcation is accompanied by the transition from three- to two-valued function, and the fourth bifurcation, at the end of the transition to resonant oscillation, is distinguished by the transition from two- to four-valued function.

Poincaré maps representing different types of LCOs are shown in Fig. 15b. Although for  $M = 1.1$  and  $M = 1.27$ , corresponding to the first mode and resonant oscillations, respectively, the map consists of two and four points (slight motion of the points from cycle to cycle occurs due to the flow unsteadiness), for  $M = 1.45, 1.56,$  and  $1.6$ , corresponding to nonperiodic oscillations, there is a cloud of points. It can be noted, however, that for  $M = 1.45$  and  $1.6$ , this cloud is not fully chaotic but is concentrated around two rings, which can signify only a small quasi-chaotic component imposed on a dominant regular motion. For  $M = 1.56$ , the cloud of points is not regular, which signifies a more pronounced quasi-chaotic component of the motion.

## IV. Results of Calculations for Decelerating Flow

### A. Slow Deceleration

The slowest flow deceleration considered in this study corresponds to  $T = 10$  s. The plate behavior in this case is significantly different from faster decelerations, that is why it is considered separately. The time history of the reference point deflection is shown in Fig. 16a.

The following changes in the plate dynamics are observed.

1) When  $M$  is decreasing, the vibrations start at  $M = 1.45$  and correspond to the first mode shape. The oscillations spectrum also shows that the first mode only is present.

2) Transition from first-mode to high-frequency nonperiodic oscillations at  $M \approx 1.39$ . Evolution of the time series and phase portrait is shown in Figs. 17a and 17b, where nonrepeatability of the oscillations from cycle to cycle is clearly seen.

3) Transition from nonperiodic oscillations to the second-mode limit-cycle oscillations at  $M \approx 1.26$ . The plate oscillates in a pure

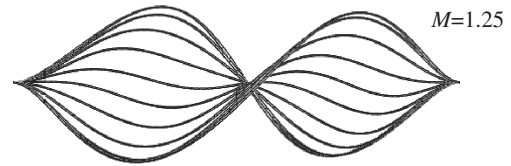


Fig. 18 Plate shapes during second-mode oscillations.

second-mode shape (Fig. 18); the corresponding frequency becomes dominant in the spectrum (Sec. IV.D). The phase portrait shown in Fig. 19 corresponds to purely sinusoidal oscillations.

4) Transition from pure second mode to resonant limit cycle occurs at  $M \approx 1.17$ . The spectrum consists of the first, second, and third modes (Sec. IV.D), exactly as in the case of accelerating and constant-speed flows. The transformation of the phase portrait is shown in Fig. 20. Oscillations lose the symmetry due to the presence of the second mode, whose frequency is two times larger than that of the first mode.

5) Transition from resonant to the first mode limit cycle occurs at  $M \approx 1.09$  (Fig. 21), and oscillations again become almost symmetrical.

6) Transition from “smooth” first-mode flutter to first-mode flutter with twists takes place at  $M = 1.06$  (Fig. 22, arrows show the directions of twist motions when  $M$  increases).

7) Transition from flutter to divergence at  $M = 1$ . Note that the plate shape is reversed at  $M \approx 0.83$ , which is caused by a slight depressurization over the plate due to continuous slowing down of the flow. That is why the plate buckling direction is changed near the bifurcation point. However, this does not signify any additional bifurcation.

8) The plate become stable at  $M \approx 0.78$ .

### B. Moderate Decelerations

Moderate flow decelerations correspond to  $T = 7.5, 5,$  and  $2.5$  s, which demonstrate similar plate dynamics. The main difference from the case of  $T = 10$  s is the absence of pure second-mode limit cycle. Otherwise, the sequence of the bifurcations in the plate dynamics is the same as for  $T = 10$  s.

A typical time history of the reference point deflection is shown in Fig. 16b. As well as for  $T = 10$  s, oscillations in the first mode start to grow at  $M = 1.45$ , followed by the transition to high-frequency nonperiodic oscillations. The latter is followed by the bifurcation to

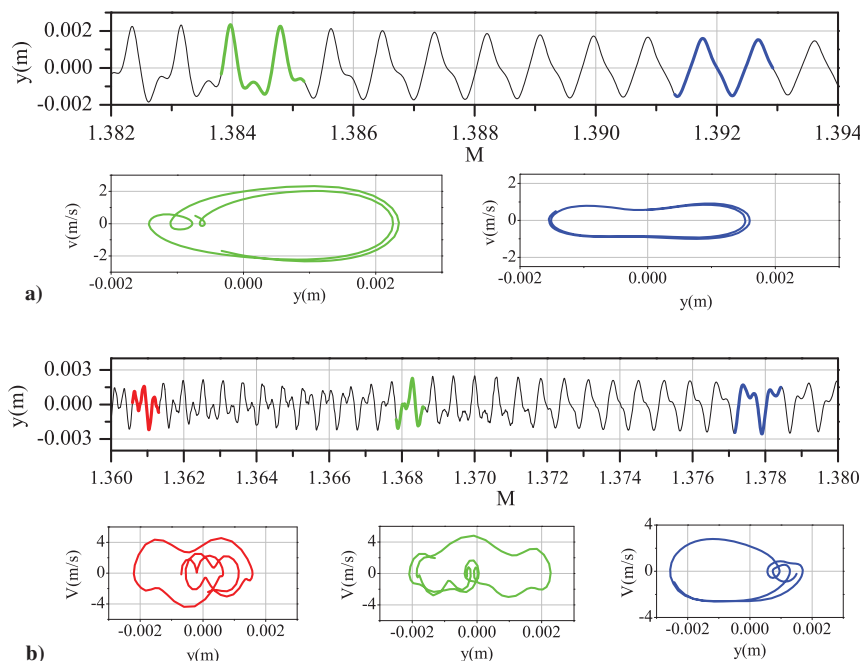
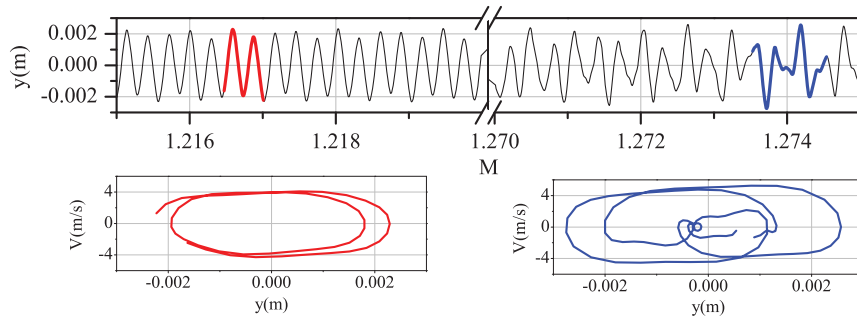
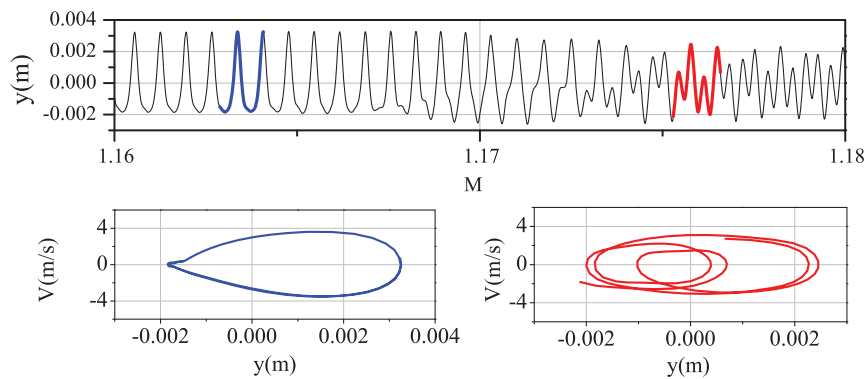


Fig. 17 Reference point deflection and phase trajectories a) for transition from the first mode to nonperiodic oscillations, and b) for evolution of nonperiodic oscillations.



**Fig. 19** Reference point deflection and phase trajectories for transition from nonperiodic oscillations to single second-mode LCOs.



**Fig. 20** Reference point deflection vs Mach number and phase diagrams for transition from pure second-mode LCOs to resonant flutter in the first and second modes.

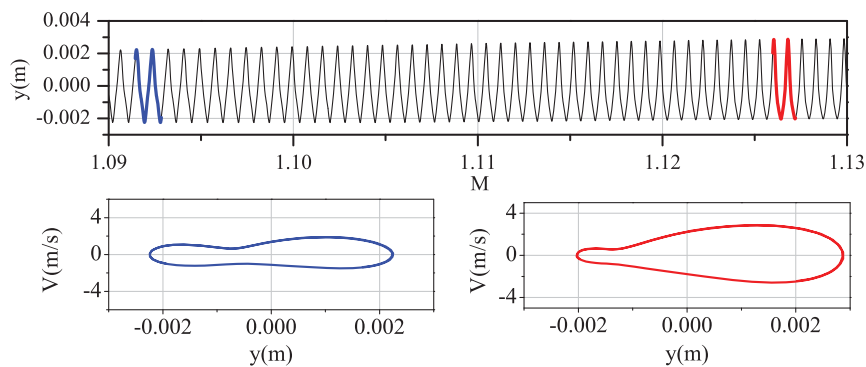


**Fig. 21** Reference point deflection vs Mach number and phase diagrams for transition from resonant flutter to first-mode flutter.

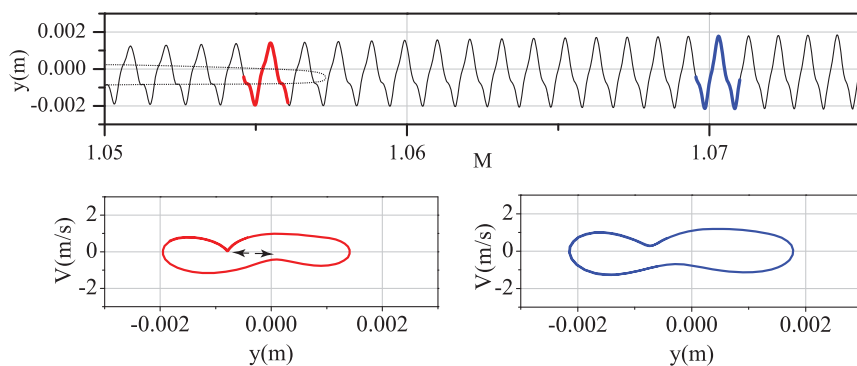


**Fig. 22** Reference point deflection vs Mach number and phase diagrams for transition from smooth first-mode LCOs to LCOs with twists.

resonant limit-cycle oscillations and then to the first-mode limit cycle at  $M \approx 1.09$ . After the appearance of twists, visible as the bifurcation in the first-mode cycle at  $M \approx 1.06$ , the plate becomes statically diverged at  $M \approx 1.0$  and stabilized at  $M \approx 0.78$ .

The range of Mach numbers  $M_{ch1} < M < M_{ch2}$ , where high-frequency oscillations occur, becomes shorter for faster decelerations. The upper boundary  $M_{ch2}$  drops from 1.39 at  $T = 10$  s to 1.28 at  $T = 2.5$  s, whereas the lower boundary  $M_{ch1}$  increases from 1.17 to 1.28. At  $T = 2.5$  s, both boundaries merge with each other, such that high-frequency oscillations are almost not visible (Fig. 16b). The explanation is similar to the same phenomenon for the accelerating flow (Sec. III.B); development of higher modes needs more time, which becomes comparable with the time passed in the region of nonperiodic oscillations. If the deceleration is sufficiently fast, nonperiodic oscillations do not have time to develop.

### C. Fast Decelerations

Fast flow decelerations correspond to  $T = 1$  and 0.5 s (Fig. 16c). Its main feature is the absence of nonperiodic oscillations, so that the first mode flutter is directly followed by resonant limit-cycle oscillations at  $M = 1.18$ . Also, for lower  $M$ , at such a high deceleration, the panel makes just a few oscillations in the first-mode regime, and its bifurcation associated with the disappearance of twists is almost not visible.

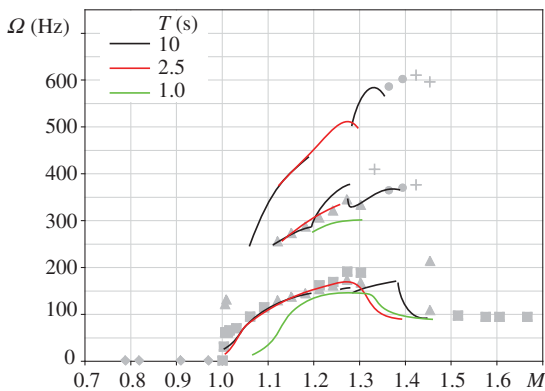


**Fig. 23** Dominant frequencies in the oscillation spectrum vs  $M$  for decelerating flow. Symbols denote results for constant-speed flow (same as in Fig. 14).

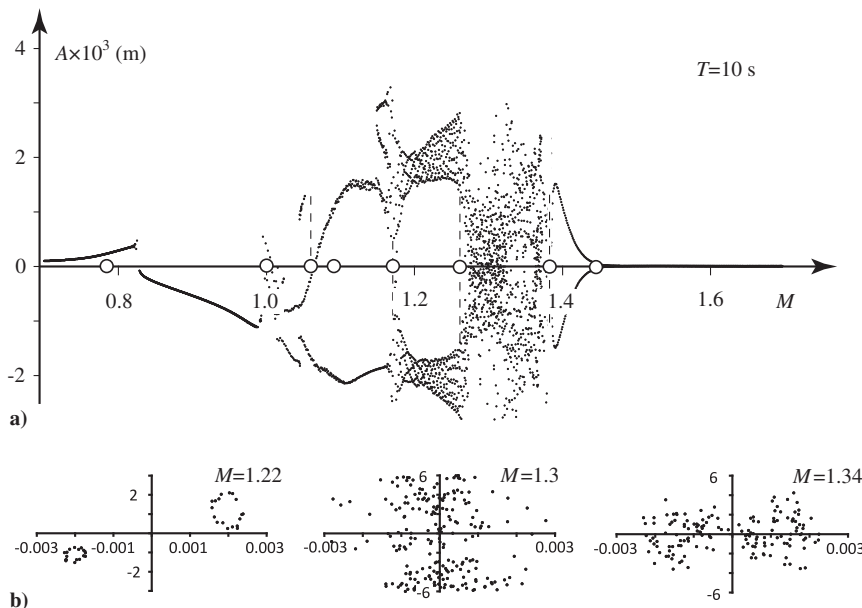


**Fig. 24** Representations of a) position of point 1 at extrema of point 2 for decelerating flow,  $T = 10$  s, and b) corresponding Poincaré maps at various Mach numbers.

### D. Oscillation Frequency

Dominant frequencies in oscillation spectrum in decelerating flow are shown in Fig. 23. As well as for accelerating flow, at the range of nonperiodic oscillations, the spectrum is very different for different decelerations due to nonuniqueness of the oscillation regime. However, for  $M < 1.2$ , when resonant and nonresonant first-mode oscillations occur, the frequencies for different decelerations are close to each other and to those for constant-speed flow.

### E. Poincaré Maps

Finally, consider point 1 deflections when the point 2 deflection reaches its extremum, shown in Fig. 24a (similar to Sec. III.E). Each bifurcation in the plate dynamics is clearly seen, as well as the region of nonperiodic oscillations. The most interesting Poincaré maps (Fig. 24b) represent the second-mode limit cycle (absent in accelerating flow) and nonperiodic oscillations. By comparing the maps with Fig. 15b, we conclude that, in decelerating flow, nonperiodic oscillations have more pronounced quasi-chaotic motion component. In particular, no regular structures (like the two-ring structure in Fig. 15b for  $M = 1.45$  and 1.6) are seen.

## V. Comparison of the Panel Response in Accelerating, Decelerating, and Constant-Speed Flows

### A. Hysteresis Loops at Acceleration and Deceleration

According to the results presented in previous sections, in the region of divergence ( $M < 1$ ), first-mode, and resonant first- and second-mode LCOs (small  $M > 1$ ), the plate dynamics is the same for different accelerations and decelerations. However, at higher Mach numbers, the plate behavior for each case is significantly different. That takes place even for small acceleration and deceleration that correspond to  $T = 10$  s (Fig. 25), for which the amplitudes and frequencies are almost the same at  $M < 1.17$ , where the instability occurs in the form of divergence as well as first-mode and resonant LCOs but become different at  $1.17 < M < 1.7$ , where higher-mode oscillations occur. This can be seen in the amplitude as well as the frequency plot (Fig. 25), where a hysteresis loop is observed. Frequencies in nonperiodic high-frequency regime for accelerating flow are close to those in constant-speed flow, but this regime is established at higher  $M$  due to time needed for the growth of high-frequency perturbations.

A similar hysteresis loop is seen at higher accelerations, for example, for  $T = 2.5$  (Fig. 26). In all cases, the hysteresis loops appear in the region of nonperiodic high-frequency oscillations

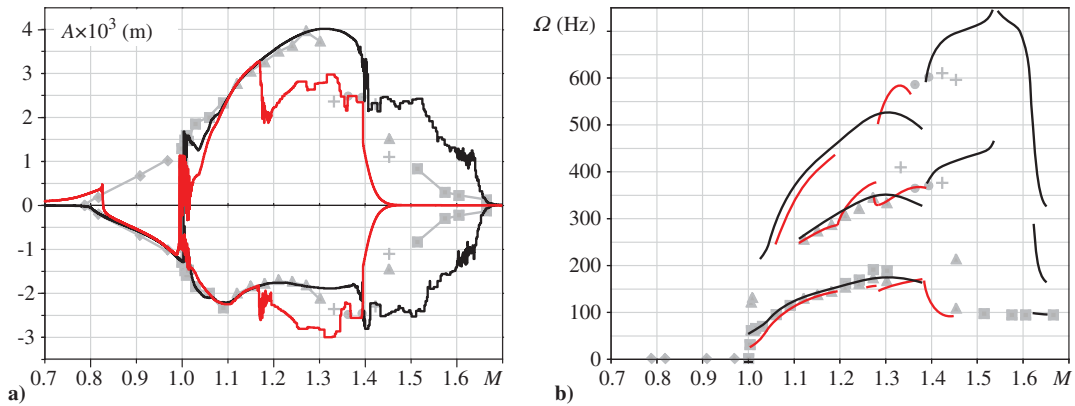


**Fig. 25** Representations of a) amplitude and b) frequency of reference point oscillation vs Mach number for acceleration (black) and deceleration (red) for  $T = 10$  s. Symbols denote results for constant-speed flow (same as in Fig. 14).

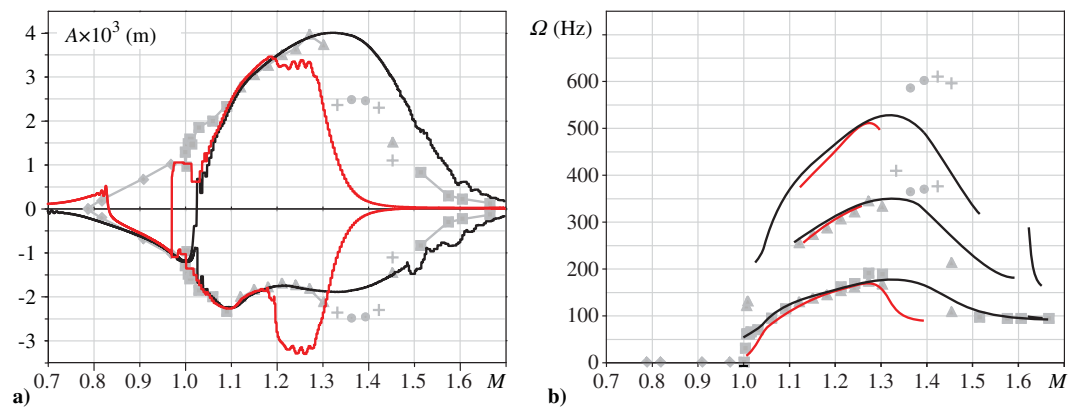


**Fig. 26** Representations of a) amplitude and b) frequency of reference point oscillation vs Mach number for acceleration (black) and deceleration (red) for  $T = 2.5$  s. Symbols denote results for constant-speed flow (same as in Fig. 14).

(acceleration and constant speed) and first-mode oscillations (deceleration), whereas the oscillation regimes coincide at resonant and nonresonant LCOs at lower  $M$ .

At higher accelerations,  $T = 1$  s (Fig. 27), there is no high-frequency nonperiodic oscillations; accordingly, the hysteresis loop occupies the region of the first-mode flutter and stability at high Mach numbers ( $1.16 < M < 1.7$ ). For  $M < 1.16$ , amplitude plots are close to each other.

### B. Comparison of Different Accelerations

Comparison of amplitudes of the typical cases of accelerations ( $T = 10, 2.5,$  and  $1$  s) is shown in Fig. 28. It is seen that, for  $M < 1.4$ , the amplitudes in all cases are close to each other and to the amplitude obtained in constant-speed flow. The difference in the amplitude appears when the oscillation type is changed from resonant LCOs to higher-mode oscillations, which occurs at Mach number that depends on the acceleration.

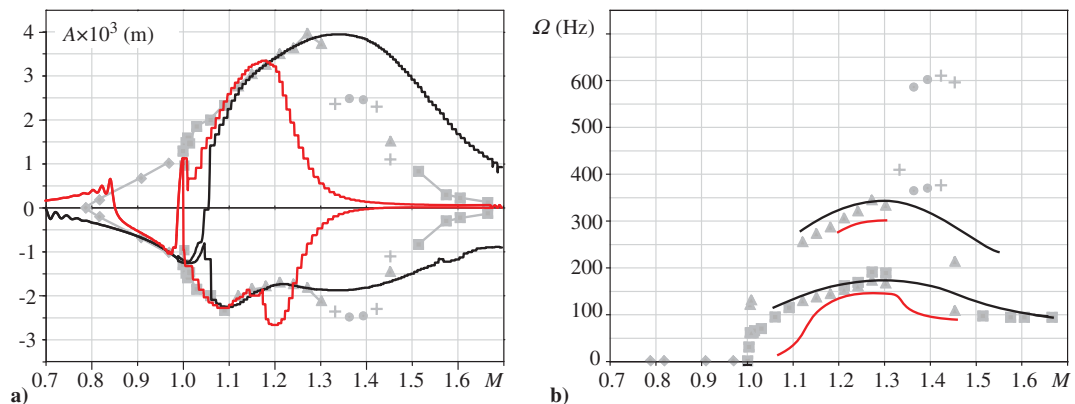


**Fig. 27** Representations of a) amplitude and b) frequency of reference point oscillation vs Mach number for acceleration (black) and deceleration (red) for  $T = 1$  s. Symbols denote results for constant-speed flow (same as in Fig. 14).

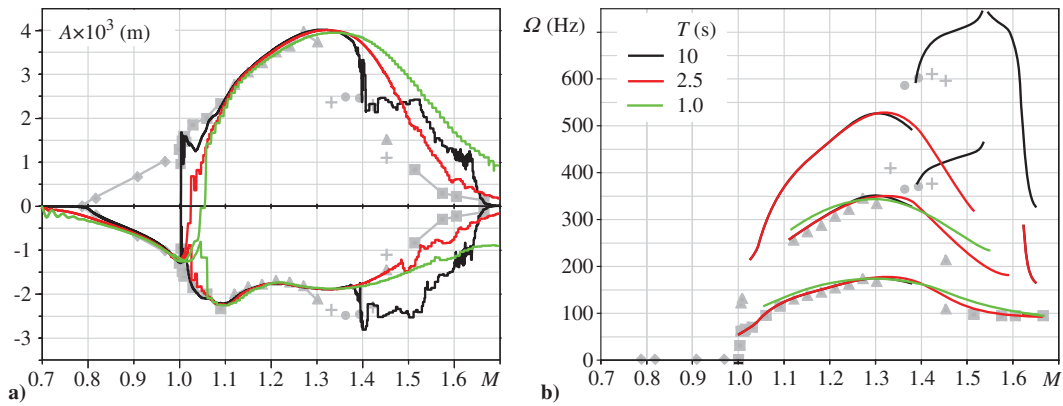


**Fig. 28** Amplitude of reference point deflection and dominant frequencies vs Mach number for different accelerations. Symbols denote results for constant-speed flow (same as in Fig. 14).

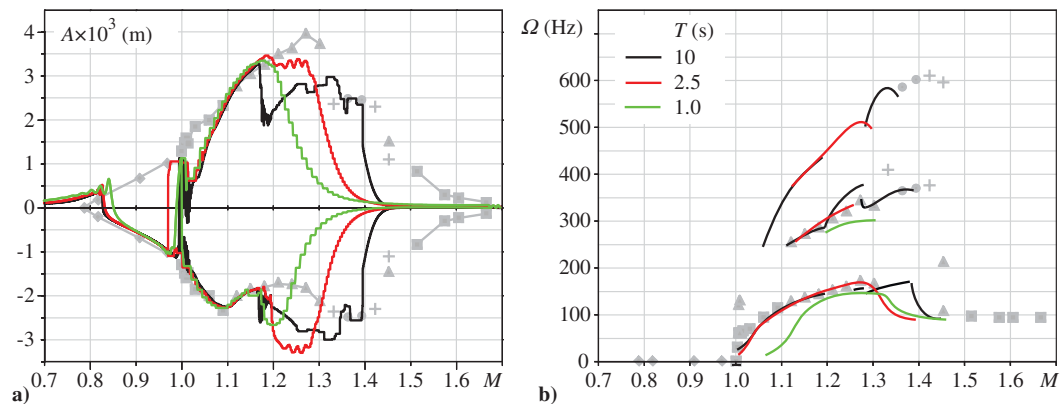


**Fig. 29** Amplitude of reference point deflection and dominant frequencies vs Mach number for different decelerations. Symbols denote results for constant-speed flow (same as in Fig. 14).

### C. Comparison of Different Decelerations

Comparison of typical decelerations ( $T = 10, 2.5, 1$  s) is shown in Fig. 29. As well as for accelerations, we conclude that the oscillations are the same in the region of divergence, first-mode and resonant LCOs at lower  $M$ . The difference appears at higher  $M$ , where the onset of oscillations is delayed for higher decelerations due to time needed for their development. It can also be noted that the initial growth of the first-mode oscillations in decelerating flow starts at  $M \approx 1.45$  for all values of deceleration.

## VI. Conclusions

From the structural safety point of view, the most dangerous type of nonlinear dynamics of skin panels is high-frequency oscillations. First, they correspond to much higher dynamic stress due to presence of higher mode shapes; second, they yield much faster accumulation of cycles due to higher frequency of oscillations. In this study, it has been shown that this type of oscillation is fully suppressed if the flow acceleration (or deceleration) is sufficiently large. For the parameters considered in this study (steel plate at sea level or aluminum plate at 11,000 m above sea level), the suppression occurs for  $T < 2.5$  s, which corresponds to the acceleration of 13g. The mechanism of the suppression is as follows: because higher-mode oscillations have very long period of formation, the flow acceleration (deceleration) becomes large enough to pass the region of high-frequency oscillations ( $1.4 < M < 1.5$ ) faster than they grow and, hence, faster than the nonlinear oscillations in higher modes are actually formed.

On the other hand, low-frequency types of oscillations, namely, pure first-mode limit-cycle oscillations and limit cycle with internal 1:2 resonance, are not sensitive to the flow acceleration (deceleration); even for extremely large accelerations ( $T = 0.5$  s corresponds to 67g), the amplitude reaches the same values as in constant-speed flow. This occurs because, unlike high-frequency oscillations, the formation of limit cycle for first-mode and resonant

oscillations occurs during 3–5 cycles of oscillations, and the panel responds to the change of the flow condition very fast. Hence, for these oscillation regimes, the only effect of faster passing through the transonic region is a lower number of cycles collected in the single-mode flutter regime but not full suppression of flutter or at least a decrease in amplitude.

### Acknowledgment

This work is supported by the grant MK-5514.2016.1 and Russian Foundation for Basic Research (project 18-01-00404).

### References

- [1] Bendiksen, O. O., "Review of Unsteady Transonic Aerodynamics: Theory and Applications," *Progress in Aerospace Sciences*, Vol. 47, No. 2, 2011, pp. 135–167. doi:10.1016/j.paerosci.2010.07.001
- [2] Bendiksen, O. O., "High-Altitude Limit Cycle Flutter of Transonic Wings," *Journal of Aircraft*, Vol. 46, No. 1, 2009, pp. 123–136. doi:10.2514/1.36413
- [3] Vedenev, V. V., "Effect of Damping on Flutter of Simply Supported and Clamped Panels at Low Supersonic Speeds," *Journal of Fluids and Structures*, Vol. 40, July 2013, pp. 366–372. doi:10.1016/j.jfluidstructs.2013.04.004
- [4] Bendiksen, O. O., "Transonic Flutter Characteristics of Advanced Fighter Wings," *56th AIAA/ASCE/AHS/ASC Structures, Structural Dynamics, and Materials Conference*, AIAA Paper 2015-0438, 2015. doi:10.2514/6.2015-0438
- [5] Shishaeva, A., Vedenev, V., and Aksenov, A., "Nonlinear Single-Mode and Multi-Mode Panel Flutter Oscillations at Low Supersonic Speeds," *Journal of Fluids and Structures*, Vol. 56, July 2015, pp. 205–223. doi:10.1016/j.jfluidstructs.2015.05.005
- [6] Bolotin, V. V., *Nonconservative Problems of the Theory of Elastic Stability*, Pergamon Press, Oxford, England, U.K., 1963.

- [7] Grigolyuk, E. I., Lamper, R. E., and Shandarov, L. G., *Flutter of Plates and Shells*, 1963, VINITI, Moscow, 1965, pp. 34–90 (in Russian).
- [8] Dowell, E. H., *Aeroelasticity of Plates and Shells*, Noordhoff International, Leyden, The Netherlands, 1974.
- [9] Novichkov, , and Yu, N., “Flutter of Plates and Shells,” *Mechanics of Deformable Solids*, Vol. 11, Progress in Science and Technology, VINITI, Moscow, 1978, pp. 67–122 (in Russian).
- [10] Mei, C., Abdel-Motagaly, K., and Chen, R. R., “Review of Nonlinear Panel Flutter at Supersonic and Hypersonic Speeds,” *Applied Mechanics Reviews*, Vol. 52, No. 10, 1999, pp. 321–332. doi:10.1115/1.3098919
- [11] Algazin, S. D., and Kijko, I. A., “Aeroelastic Vibrations and Stability of Plates and Shells,” *De Gruyter Studies in Mathematical Physics*, Vol. 25, Walter de Gruyter, Berlin, 2014.
- [12] Shitov, S., and Vedeneev, V., “Flutter of Rectangular Simply Supported Plates at Low Supersonic Speeds,” *Journal of Fluids and Structures*, Vol. 69, Feb. 2017, pp. 154–173. doi:10.1016/j.jfluidstructs.2016.11.014
- [13] Vedeneev, V. V., “On the Application of the Asymptotic Method of Global Instability in Aeroelasticity Problems,” *Proceedings of the Steklov Institute of Mathematics*, Vol. 295, No. 1, 2016, pp. 274–301. doi:10.1134/S0081543816080174
- [14] Bendiksen, O. O., and Davis, G. A., “Nonlinear Traveling Wave Flutter of Panels in Transonic Flow,” *36th Structures, Structural Dynamics and Materials Conference*, AIAA Paper 1995-1486, 1995. doi:10.2514/6.1995-1486
- [15] Gordnier, R. E., and Visbal, M. R., “Development of a Three-Dimensional Viscous Aeroelastic Solver for Nonlinear Panel Flutter,” *Journal of Fluids and Structures*, Vol. 16, No. 4, 2002, pp. 497–527. doi:10.1006/jfls.2000.0434
- [16] Hashimoto, A., Aoyama, T., and Nakamura, Y., “Effect of Turbulent Boundary Layer on Panel Flutter,” *AIAA Journal*, Vol. 47, No. 12, 2009, pp. 2785–2791. doi:10.2514/1.35786
- [17] Mei, G., Zhang, J., Xi, G., Sun, X., and Chen, J., “Analysis of Supersonic and Transonic Panel Flutter Using a Fluid–Structure Coupling Algorithm,” *Journal of Vibration and Acoustics*, Vol. 136, No. 3, 2014, Paper 031013. doi:10.1115/1.4027135
- [18] Alder, M., “Development and Validation of a Fluid–Structure Solver for Transonic Panel Flutter,” *AIAA Journal*, Vol. 53, No. 12, 2015, pp. 3509–3521. doi:10.2514/1.J054013
- [19] Alder, M., “Nonlinear Dynamics of Pre-Stressed Panels in Low Supersonic Turbulent Flow,” *AIAA Journal*, Vol. 54, No. 11, 2016, pp. 3632–3646. doi:10.2514/1.J054783
- [20] Hejranfar, K., and Azampour, M. H., “Simulation of 2D Fluid–Structure Interaction in Inviscid Compressible Flows Using a Cell-Vertex Central Difference Finite Volume Method,” *Journal of Fluids and Structures*, Vol. 67, Nov. 2016, pp. 190–218. doi:10.1016/j.jfluidstructs.2016.09.009
- [21] Mei, G., Zhang, J., and Kang, C., “Analysis of Curved Panel Flutter in Supersonic and Transonic Airflows Using a Fluid–Structure Coupling Algorithm,” *Journal of Vibration and Acoustics*, Vol. 139, No. 4, 2017, Paper 041004. doi:10.1115/1.4036103
- [22] Muhlstein, L., Jr., Gaspers, P. A., Jr., and Riddle, D. W., “An Experimental Study of the Influence of the Turbulent Boundary Layer on Panel Flutter,” NASA TN D-4486, 1968.
- [23] Gaspers, P. A., Jr., Muhlstein, L., Jr., and Petroff, D. N., “Further Results on the Influence of the Turbulent Boundary Layer on Panel Flutter,” NASA TN D-5798, 1970.
- [24] Dowell, E. H., “Generalized Aerodynamic Forces on a Flexible Plate Undergoing Transient Motion in a Shear Flow with an Application to Panel Flutter,” *AIAA Journal*, Vol. 9, No. 5, 1971, pp. 834–841. doi:10.2514/3.6283
- [25] Dowell, E. H., “Aerodynamic Boundary Layer Effect on Flutter and Damping of Plates,” *Journal of Aircraft*, Vol. 10, No. 12, 1973, pp. 734–738. doi:10.2514/3.60298
- [26] Vedeneev, V., “Interaction of Panel Flutter with Inviscid Boundary Layer Instability in Supersonic Flow,” *Journal of Fluid Mechanics*, Vol. 736, Dec. 2013, pp. 216–249. doi:10.1017/jfm.2013.522
- [27] Bondared, V., and Vedeneev, V., “Short-Wave Instability of an Elastic Plate in Supersonic Flow in the Presence of the Boundary Layer,” *Journal of Fluid Mechanics*, Vol. 802, Sept. 2016, pp. 528–552. doi:10.1017/jfm.2016.482
- [28] Vedeneev, V. V., “Nonlinear High-Frequency Flutter of a Plate,” *Fluid Dynamics*, Vol. 42, No. 5, 2007, pp. 858–868. doi:10.1134/S0015462807050183
- [29] Vedeneev, V. V., “Limit Oscillatory Cycles in the Single Mode Flutter of a Plate,” *Journal of Applied Mathematics and Mechanics*, Vol. 77, No. 3, 2013, 257–267. doi:10.1016/j.jappmathmech.2013.09.001
- [30] Xie, D., Xu, M., Dai, H., and Dowell, E. H., “Observation and Evolution of Chaos for a Cantilever Plate in Supersonic Flow,” *Journal of Fluids and Structures*, Vol. 50, Oct. 2014, pp. 271–291. doi:10.1016/j.jfluidstructs.2014.05.015

M. Smith  
Associate Editor